Systematics of Neutron Separation Energies*

K. N. GELLER, J. HALPERN, AND E. G. MUIRHEAD†
Physics Department, University of Pennsylvania, Philadelphia, Pennsylvania
(Received December 14, 1959)

Photoneutron thresholds for 73 isotopes have been measured by radioactivity and neutron detection methods using a 25-Mev betatron. The neutron separation energies inferred from the observed thresholds are in general agreement with the values predicted from mass data and reaction energies. Several discrepancies are observed between threshold and neutron binding energies where ground state transitions require a spin change $\geqslant 7/2$. For these nuclei, the threshold energies are consistent with neutron emission leaving the residual nucleus in an excited state.

INTRODUCTION

IN addition to mass spectroscopic measurements, and beta and alpha disintegration energies, nuclear reaction energies furnish valuable information regarding nuclear masses and binding energies. In particular, from the measured Q value for reactions where the initial and residual nuclei differ by one neutron, one can evaluate the binding energy and mass difference between neighboring isotopes. The neutron pairing energy, which is related to the strength of the two particle interaction, can be obtained from the difference in neutron binding energies between neighboring isotopes of even and odd N.

The binding energy of the last neutron in a nucleus may be obtained from reactions which measure (1) the energy released upon the addition of a neutron to a stable nucleus, or (2) the separation energy necessary to remove a neutron from a stable nucleus. Accordingly, reactions of group (1) measure the binding energy of the $(A+1)$ residual nucleus, whereas group (2) of the A initial nucleus. If the transition observed is not to the ground state of the final nucleus, the neutron binding energy inferred from reaction Q values of group (1) represent a lower limit to the true value while the reaction Q value of group (2) represent an upper limit.

Although neutron binding energies may be ascertained by several types of reactions belonging to either of the above two groups, they are quite readily and accurately obtained from neutron separation energies measured with high-energy x radiation from a betatron. The reaction yield in this case is given by the integrated product of the (γ,n) cross section and the incident photon spectrum. The neutron separation energy is defined as the threshold for the (γ,n) reaction. To determine the (γ,n) threshold, one measures the neutron yield as a function of peak bremsstrahlung energy and then extrapolates to zero yield. The experimental uncertainty in the threshold determination will depend on the accuracy with which the betatron energy is known, and the sensitivity available for detecting the neutron yield. The detection sensitivity, which depends on instrumental factors as well as the shape of the (γ,n) cross section at threshold, determines the energy definition with which the neutron yield curve can sensibly be measured. This in turn limits the accuracy associated with the threshold extrapolation. Whereas the early experimental results of Baldwin and Koch[1] quoted errors of about 4% for the observed threshold energies, improved techniques now make it possible to measure thresholds to better than 0.5%.[2–5]

A significant improvement in betatron operation has been the ability to control the peak bremsstrahlung energy to a high degree of accuracy; energy stability of ± 5 kev over periods of several hours, and ± 20 kev over periods of several days have been achieved. Unfortunately, however, although energy stability to this degree of accuracy is possible, rather large uncertainties in the assignment of a precise value for the betatron energy still persist. Most betatron energy scales are established empirically by comparing measured photoneutron thresholds with Q values predicted from mass data and reaction energies. This procedure requires that the experimentally observed threshold correspond to the true threshold and the Q value be accurately known. There has been some doubt as to whether both of these requirements have been satisfied, especially in the region of light nuclei. Thus, betatron energy scales referred to C^{12}, N^{14}, O^{16}, and F^{19} as calibration standards are subject to re-examination. This point is discussed to some extent in reference 5.

The reaction threshold, defined as the energy at which the reaction yield is zero, must always be inferred by extrapolation of the measured yield data. Early experimental results indicated that the relative neutron yield in the region of threshold could be represented by $Y(E_b)\alpha(E_b-E_{th})^m$, where E_b and E_{th}

* This work supported in part by the U. S. Air Research and Development and a joint program of the Office of Naval Research and the U. S. Atomic Energy Commission.
† Fulbright Fellow; permanent address: University of Melbourne, Melbourne, Australia.

[1] G. C. Baldwin and H. W. Koch, Phys. Rev. **67**, 1 (1945).
[2] R. A. Tobin, J. McElhinney, and L. Cohen, Phys. Rev. **110**, 1388 (1958).
[3] W. L. Bendel, J. McElhinney, and R. A. Tobin, Phys. Rev. **111**, 1297 (1958).
[4] B. G. Chidley, L. Katz, and S. Kowalski, Can. J. Phys. **36**, 407 (1958).
[5] A. S. Penfold and E. L. Garwin, Phys. Rev. **115**, 420 (1959).

are the x ray and threshold energies, respectively, and the exponent m a constant.[6] This approach was predominantly based on yield data considerably removed from threshold and taken in energy increments of about 200 kev. Under these conditions, the simple energy dependence experimentally observed was assumed valid in the immediate vicinity of threshold. Log-log and square root plots of the yield data proved quite successful in determining a unique value of the threshold, but there was little theoretical justification that the values predicted were the true values for the neutron separation energies. Axel and Fox[7] in discussing this problem conclude that the form $(E_b-E_{th})^m$ is only valid over a limited region of the yield curve. More recently, it has been demonstrated by Chidley et al.[4] that threshold energies obtained by a simple power law extrapolation are from 20 to 60 kev lower than what one obtains from visual inspection of yield data taken in the immediate vicinity of threshold. This conclusion is also borne out by the present results.

In view of these findings concerning calibration uncertainties and threshold interpretation, it seemed desirable to reexamine the threshold measurements with reference to an energy scale which did not include any light elements as standards. To improve the accuracy in defining the threshold, yield data in the vicinity of threshold were measured in energy increments of 27 kev or better for most cases. A total of 73 photoneutron thresholds were measured throughout the periodic table with an average accuracy of 50 kev. With the exception of carbon, nitrogen, oxygen, and fluorine (to be published), all results are presented in the present paper and summarized in Table I. Several new threshold energies are reported in the region of the rare earth nuclides.

EXPERIMENTAL PROCEDURES

Neutron yield data in the region of the (γ,n) threshold were for the most part obtained by direct neutron detection using $B^{10}F_3$ counters embedded in paraffin.[8] The experimental arrangement is shown in Fig. 1. The x rays produced at the betatron target passed through the doughnut wall and impinged upon a thin walled aluminum ionization chamber used to monitor the integrated x ray exposure. The x ray beam was defined by a tapered lead collimator 8 in. long which limited the beam-spot size at the sample position to $\frac{7}{8}$ in. A steel clearance collimator (13-in.×15-in. with 1-in. hole) placed directly in front of the lead collimator shielded material in the direction of the beam from x-ray bombardment. This in effect reduced the photo-induced neutron background, particularly from the lead shielding walls, for betatron energies below 10 Mev. At energies greater than 10 Mev, the neutron background increased markedly with betatron energy due to photoneutron production in the copper magnet coils. The neutron detector was shielded from the betatron area by a 2 foot thick concrete wall, and located approximately 11 feet from the betatron target.

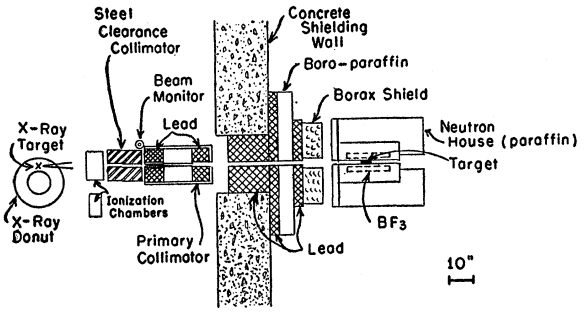

FIG. 1. Experimental arrangement for direct detection of neutrons.

The photoneutrons emitted by the irradiated sample were moderated in the paraffin medium and detected by 3 $B^{10}F_3$ counters (96% enriched in B^{10}) surrounding the target placed in a $1\frac{1}{4}$-in. opening passing through the entire length of the paraffin block. For 1 cm of paraffin between the sample and counters, the neutron population at the counter region decayed exponentially in time following the x-ray burst with a mean lifetime of about 80 microseconds. Only those pulses corresponding to neutrons reaching the counters during the interval from 12 to 800 μsec following the 0.5 μsec x-ray burst were recorded.[8] The detection efficiency for neutrons with energies less than 0.5 Mev was roughly 13%.

Samples of high purity and natural isotopic abundance were contained in aluminum cylinders, $1\frac{1}{4}$ in. in diameter and sealed with aluminum caps 5 mil thick. The amount of sample varied depending on availability, but for most measurements exceeded 50 grams. Where small quantities of sample were used, as in the rare earths, the entire sample was placed in the x-ray beam.

Neutron yields from phosphorus, potassium, praseodymium and tantalum, were measured by induced radioactivity. The samples were irradiated for a fixed integrator charge Q at a distance of 25 cm from the betatron target. An electronic integrator with time-constant set equal to the residual half-life monitored the integrated x-ray dose. The measured activity yields per unit monitor response were thus independent of fluctuations in the beam intensity. The irradiation time was adjusted for at least one half-life, except in the case of tantalum, by adjusting the input sensitivity of the recorder used to register the integrator charge. Two NaI(Tl) crystals, $1\frac{3}{4}$-in.×1-in., detected the annihilation radiation resulting from the positron

[6] J. McElhinney et al., Phys. Rev. **75**, 542 (1949); A. O. Hanson et al., Phys. Rev. **76**, 578 (1949); P. Parsons and C. Collie, Proc. Phys. Soc. (London) **A63**, 839 (1950); R. Sher, J. Halpern, and A. K. Mann, Phys. Rev. **84**, 387 (1951); M. Birnbaum, Phys. Rev. **93**, 146 (1954).

[7] P. Axel and J. Fox, Phys. Rev. **102**, 400 (1956).

[8] J. Halpern, A. K. Mann, and R. Nathans, Rev. Sci. Instr. **23**, 678 (1952).

TABLE I. Summary and comparison of neutron separation energies inferred from present threshold measurements with values predicted from mass data and reaction energies. All energies are expressed in the center-of-mass system in Mev.

Reaction	No. runs	Present results	Other results	Method	Reference
$D^2(\gamma,n)H^1$	10	2.226±0.001 (calib)	2.226±0.001	LSA	a
$C^{12}(\gamma,\gamma)C^{12}$	1	15.115±0.006 (calib)	15.116±0.006	$B^{11}(d,n\gamma_{15})C^{12}$	b
$Al^{27}(\gamma,n)Al^{26}$	2	13.26 ±0.07 (13.03)	13.06 ±0.06	LSA	c
			13.057±0.011	mass data	d
				$Q(\beta+)$	c
			13.038±0.015	reaction cycle	e
			12.98 ±0.08	threshold	f
$P^{31}(\gamma,n)P^{30}$	5	$\leqslant$12.391±0.026	12.40 ±0.08	LSA	c
			12.391±0.030	LSA	a
			12.359±0.017	reaction cycle	e
			12.321±0.009	mass data	g
			12.50 ±0.05	threshold	f
$Cl^{37}(\gamma,n)Cl^{36}$	1	10.307±0.037	10.322±0.023	LSA	h
			10.316±0.004	mass data	g
$K^{39}(\gamma,n)K^{38}$	1	$\leqslant$13.125±0.038	13.089±0.033	LSA	h
(to 7.7-min state)			13.087±0.011	mass data	g
$V^{51}(\gamma,n)V^{50}$	1	11.04 ±0.06	11.040±0.004	mass data	g
			11.16 ±0.05	threshold	f
$Cr^{52}(\gamma,n)Cr^{51}$	1	$\leqslant$12.18 ±0.14	12.053±0.004	mass data	g
$Cr^{53}(\gamma,n)Cr^{52}$	1	7.92 ±0.06	7.946±0.007	$Cr^{52}(d,p)Cr^{53}$	i
			7.943±0.004	mass data	g
$Mn^{55}(\gamma,n)Mn^{54}$	13	10.192±0.020	10.209±0.007	mass data	g
			10.14±0.05	threshold	f
$Fe^{56}(\gamma,n)Fe^{55}$	1	11.25 ±0.06	11.159±0.028	mass data	j
			11.34 ±0.10	threshold	k
$Fe^{57}(\gamma,n)Fe^{56}$	1	7.85 ±0.13	7.633±0.007	mass data	j
			7.636±0.010	$Fe^{56}(n,\gamma)Fe^{57}$	e
			7.85 ±0.13	threshold	k
$Co^{59}(\gamma,n)Co^{58}$	4	10.441±0.026	10.490±0.010	mass data	j
			10.44 ±0.05	threshold	f
$Cu^{63}(\gamma,n)Cu^{62}$	3	10.833±0.017 (calib)	10.826±0.018	mass data	j
$Cu^{65}(\gamma,n)Cu^{64}$	2	9.896±0.028	9.913±0.006	mass data	j
			9.89 ±0.11	threshold	l
$Ga^{71}(\gamma,n)Ga^{70}$	1	9.24 ±0.06	9.22 ±0.16	mass data	m
				$Q(\beta^+)$	n
$As^{75}(\gamma,n)As^{74}$	4	10.259±0.031	10.11 ±0.16	mass data	m
				$Q(\beta^+)$	o
			10.14 ±0.13	mass data	m
				$Q(\beta^-)$	o
			10.24 ±0.08	threshold	f
$Br^{81}(\gamma,n)Br^{80}$	1	10.130±0.035	10.03 ±0.13	mass data	m
				$Q(\beta^-)$	n
			10.03 ±0.13	mass data	m
				$Q(\beta^+)$	o
$Rb^{85}(\gamma,n)Rb^{84}$	1	10.65 ±0.08	10.26 ±0.16	mass data	m
				$Q(\beta^+)$	n
			10.13 ±0.25	mass data	m
				$Q(\beta^-)$	n
$Rb^{87}(\gamma,n)Rb^{86}$	1	9.99 ±0.07	9.91 ±0.20	mass data	m
				$Q(\beta^-)$	n
			9.89 ±0.05	threshold	k
$Y^{89}(\gamma,n)Y^{88}$	3	$\leqslant$11.59 ±0.08	11.53 ±0.40	mass data	m
				$Q(\beta^+)$	n
			11.82 ±0.05	threshold	f
$Nb^{93}(\gamma,n)Nb^{92}$	2	8.78±0.06	$\geqslant$8.61 ±0.52	mass data	m
				$Q(\epsilon)$	n
			8.86 ±0.05	threshold	f

[a] J. Mattauch, L. Waldmann, R. Bieri, and F. Everling, *Annual Review of Nuclear Science* (Annual Reviews, Inc., Palo Alto, 1956), Vol. 6, p. 179.
[b] R. W. Kavanagh and C. A. Barnes, Phys. Rev. **112**, 503 (1958).
[c] A. H. Wapstra, Physica **21**, 367 (1955).
[d] T. T. Scolman, K. S. Quisenberry, and A. O. Nier, Phys. Rev. **102**, 1076 (1956).
[e] P. M. Van Patter and W. Whaling, Revs. Modern Phys. **26**, 402 (1954); **29**, 756 (1957).
[f] See reference 4.
[g] C. F. Giese and J. L. Benson, Phys. Rev. **110**, 712 (1958).
[h] P. M. Endt et al., Phys. Rev. **105**, 1002 (1957).
[i] M. Mazari, W. W. Buechner, and A. Sperduto, Phys. Rev. **112**, 1691 (1958).
[j] K. S. Quisenberry, T. T. Scolman, and A. O. Nier, Phys. Rev. **104**, 461 (1956).
[k] See reference 2.
[l] See reference 3.
[m] Henry E. Duckworth, *Mass Spectroscopy* (Cambridge University Press, New York, 1958), p. 177.
[n] L. J. Lidofsky, Revs. Modern Phys. **29**, 773 (1957).
[o] R. W. King, Revs. Modern Phys. **26**, 327 (1954).
[p] W. H. Johnson, Jr., and A. O. Nier, Phys. Rev. **105**, 1014 (1957).
[q] W. H. Johnson, Jr., and V. B. Bhanot, Phys. Rev. **107**, 6 (1957).
[r] J. L. Benson, R. A. Damerow, and R. R. Ries, Phys. Rev. **113**, 1105 (1959).
[s] J. R. Huizenga, Physica **21**, 410 (1955).
[t] M. T. McEllistrem et al., Phys. Rev. **111**, 1636 (1958).

TABLE I. (*Continued*)

Reaction	No. runs	Present results	Other results	Method	Reference
$Rh^{103}(\gamma,n)Rh^{102}$	2	9.307±0.032	9.40 ±0.33	mass data	m
				$Q(\beta^+)$	n
			9.46 ±0.30	mass data	m
				$Q(\beta^-)$	n
			9.46 ±0.08	threshold	f
$Ag^{107}(\gamma,n)Ag^{106}$	2	9.353±0.034	9.38 ±0.46	mass data	m
				$Q(\beta^+)$	o
			9.43 ±0.05	threshold	l
$Ag^{109}(\gamma,n)Ag^{108}$	2	9.196±0.026	9.12 ±0.46	mass data	m
				$Q(\beta^-)$	n
			9.14 ±0.05	threshold	l
$In^{115}(\gamma,n)In^{114}$	2	9.216±0.029(9.025)	9.35 ±0.43	mass data	m
				$Q(\beta^+)$; $Q(\beta^-)$	n
			9.03 ±0.10	threshold	l
$Sb^{121}(\gamma,n)Sb^{120}$	1	9.31 ±0.06	9.27 ±0.23	mass data	m
				$Q(\beta^+)$	o
$Sb^{123}(\gamma,n)Sb^{122}$	1	8.98 ±0.05	8.95 ±0.33	mass data	m
				$Q(\beta^+)$	n
			8.98 ±0.40	mass data	m
				$Q(\beta^-)$	n
$Te^{125}(\gamma,n)Te^{124}$	1	6.56 ±0.06	6.52 ±0.39	mass data	m
			6.48 ±0.07	$Te^{124}(d,p)Te^{125}$	e
$Te^{126}(\gamma,n)Te^{125}$(?)	1	8.84 ±0.12	8.99 ±0.42	mass data	m
$Te^{128,130}(\gamma,n)Te^{127,129}$(?)	1	8.41 ±0.12	8.53 ±0.52	mass data	m
				$Q(\beta^-)$	n
			7.93 ±0.44	mass data	m
				$Q(\beta^-)$	n
$I^{127}(\gamma,n)I^{126}$	4	9.135±0.022	9.27 ±0.36	mass data	m
				$Q(\beta^-)$	n
			9.38 ±0.36	mass data	m
				$Q(\beta^+)$	n
			9.14 ±0.05	threshold	f
$Cs^{133}(\gamma,n)Cs^{132}$	2	8.988±0.033	9.03 ±0.19	mass data	p
			9.11 ±0.05	threshold	f
$Ba^{137}(\gamma,n)Ba^{136}$	1	6.949±0.038	6.99 ±0.09	mass data	p
$La^{139}(\gamma,n)La^{138}$	4	8.775±0.025	8.73 ±0.19	mass data	p
			8.81 ±0.05	threshold	f
$Pr^{141}(\gamma,n)Pr^{140}$	4	9.361±0.023	9.30 ±0.06	mass data	p
			9.46 ±0.05	threshold	f
$Ce^{142}(\gamma,n)Ce^{141}$	1	$\leqslant$ 7.24 ±0.07	6.97 ±0.07	mass data	p
$Nd^{145}(\gamma,n)Nd^{144}$	1	$\leqslant$ 6.38 ±0.16	5.97 ±0.19	mass data	p
$Sm^{149}(\gamma,n)Sm^{148}$	1	6.45 ±0.16(5.89)	5.87 ±0.28	mass data	p
$Eu^{151}(\gamma,n)Eu^{150}$	1	8.04 ±0.11			
$Eu^{153}(\gamma,n)Eu^{152}$	1	8.65 ±0.13	8.66 ±0.37	mass data	p
$Gd^{157}(\gamma,n)Gd^{156}$	1	6.39 ±0.11	6.32 ±0.06	mass data	q
$Tb^{159}(\gamma,n)Tb^{158}$	3	8.141±0.039	8.16 ±0.05	threshold	f
$Dy^{163}(\gamma,n)Dy^{162}$	1	6.32 ±0.11	6.27 ±0.06	mass data	q
$Ho^{165}(\gamma,n)Ho^{164}$	1	8.16 ±0.08	8.10 ±0.05	threshold	f
$Er^{167}(\gamma,n)Er^{166}$	1	6.64 ±0.08(6.56)	6.45 ±0.06	mass data	q
$Tm^{169}(\gamma,n)Tm^{168}$	2	8.11 ±0.05	8.00 ±0.05	threshold	f
$Yb^{173}(\gamma,n)Yb^{172}$	1	6.50 ±0.08	6.35 ±0.06	mass data	q
$Lu^{175}(\gamma,n)Lu^{174}$	1	7.88 ±0.08			
$Hf^{177}(\gamma,n)Hf^{176}$	1	6.692±0.034(6.606)	6.28 ±0.06	mass data	q
			6.70 ±0.09	threshold	k
$Hf^{179}(\gamma,n)Hf^{178}$	1	6.31 ±0.07(6.21)	6.17 ±0.06	mass data	q
			6.52 ±0.12	threshold	k
$Hf^{180}(\gamma,n)Hf^{179}$	1	7.85 ±0.11(7.48)	7.32 ±0.06	mass data	q
$Ta^{181}(\gamma,n)Ta^{180}$	5	7.640±0.025	7.66 ±0.05	threshold	f
$Ta^{181}(\gamma,n)Ta^{180}$ (to 8.1-hr state)	2	7.852±0.026			
$W^{183}(\gamma,n)W^{182}$	1	6.29 ±0.05	6.29 ±0.06	mass data	q
$W^{186}(\gamma,n)W^{185}$	1	7.28 ±0.06			
$Re^{187}(\gamma,n)Re^{186}$	1	7.18 ±0.08			
$Ir^{193}(\gamma,n)Ir^{192}$	1	7.79 ±0.05			
$Pt^{195}(\gamma,n)Pt^{194}$	2	6.205±0.044	6.09 ±0.06	mass data	q
			6.07 ±0.04	$Pt^{194}(n,\gamma)Pt^{195}$	e
$Pt^{196}(\gamma,n)Pt^{195}$	2	8.29 ±0.14	7.91 ±0.06	mass data	q
			7.920±0.012	$Pt^{195}(n,\gamma)Pt^{196}$	e
$Au^{197}(\gamma,n)Au^{196}$	3	8.057±0.022	7.96 ±0.07	threshold	f
$Hg^{199}(\gamma,n)Hg^{198}$	1	6.59 ±0.09	6.680±0.011	mass data	r
			6.68 ±0.06	mass data	q
$Hg^{201}(\gamma,n)Hg^{200}$	1	6.21 ±0.07	6.234±0.011	mass data	r
			6.27 ±0.06	mass data	q

TABLE I. (*Continued*)

Reaction	No. runs	Present results	Other results	Method	Reference
$Hg^{202}(\gamma,n)Hg^{201}$	1	7.60 ±0.13	7.760±0.011	mass data	r
			7.77 ±0.06	mass data	q
$Tl^{205}(\gamma,n)Tl^{204}$	1	7.515±0.029	7.62 ±0.17	LSA	s
$Pb^{206}(\gamma,n)Pb^{205}$	1	8.09 ±0.07	8.10 ±0.05	LSA	s
			8.09 ±0.1	$Pb^{206}(d,t)Pb^{205}$	e
$Pb^{207}(\gamma,n)Pb^{206}$	3	6.790±0.023	6.734±0.008	$Pb^{206}(n,\gamma)Pb^{207}$	e
			6.75 ±0.06	mass data	q
			6.736±0.020	$Pb^{206}(d,p)Pb^{207}$	t
			6.722±0.012	mass data	r
$Pb^{208}(\gamma,n)Pb^{207}$	3	7.404±0.028	7.36 ±0.05	$Pb^{208}(d,t)Pb^{207}$	e
			7.380±0.008	$Pb^{207}(n,\gamma)Pb^{208}$	e
			7.38 ±0.06	mass data	q
			7.357±0.012	mass data	r
$Bi^{209}(\gamma,n)Bi^{208}$	42	7.432±0.010(calib)	7.430±0.050	LSA	s

active residuals P^{30}(2.55 min), K^{38}(7.7 min) and Pr^{140}(3.4 min). Each NaI(Tl) crystal was optically coupled to the face of Dumont 6292 phototubes with a thin layer of petroleum jelly. The two detectors were mounted axially in a vertical position with a separation between crystal faces of $1\frac{3}{4}$ in. The detection system was housed in a steel enclosure with 8-in. thick walls in addition to 4 in. of lead on top of the structure. All pulses corresponding to photon absorption in the crystals greater than 60 kev were recorded. In the case of K^{38}, the annihilation radiation was counted in coincidence to reduce the background from the naturally occurring beta activity in K^{40}. A single NaI detector was used to measure the 100-kev gamma rays emitted in the decay of the 8.1-hour isomer of Ta^{180} to excited states in Hf^{180} and W^{180}.

TREATMENT OF YIELD DATA

In most cases, neutron yields were measured as a function of bremsstrahlung end-point energy in intervals of 14 or 27 kev. The energy definition, however, was much poorer (about 70 kev) where the relative neutron yield near threshold was small due to insufficient sample. A significant number of yield points were measured at energies below threshold to define the average background. This is particularly important where the neutron background is energy dependent as in the case of aluminum and other light elements (see Fig. 5). Since the determination of the (γ,n) threshold was of sole concern, corrections were not applied to the yield data for x-ray and neutron absorption in the target, variation with betatron energy of the monitor response or detector sensitivity, and counting loss.

The neutron yield data were fitted with a reasonable smooth curve and the threshold defined by the zero-slope intercept with the background. The experimental uncertainty in the extrapolated value is given by the energy increment at which the net yield and its statistical error are equal. In some instances where isotopic abundances were favorable, it was possible to resolve threshold energies for more than one isotope of a given element. The accuracy associated with the higher threshold was limited by the rising neutron yield from (γ,n) in other isotopes having lower thresholds. The following empirical procedure was applied to determine threshold energies from multi-isotopic elements: A square root plot of the measured yields was found to be linear for betatron energies about 200 kev above the lowest threshold. The neutron yield from isotopes having lower thresholds was extrapolated with a quadratic energy dependence. The higher threshold was defined by the energy at which the yield data departed from a quadratic energy dependence. This procedure is illustrated in Fig. 2, which is a plot of the yield data for lead, and the square-root of the yields. It is evident from Fig. 2 that the lowest threshold due to Pb^{207} predicted by extrapolating the square-root plot to zero yield is about 60 kev less than what is obtained from the yield data in the immediate vicinity of threshold.

Isotopic assignment of the observed thresholds is based on general nuclear stability considerations as embodied in the semiempirical mass formula.[9]

To check the subjectivity inherent in the extrapolation procedure to define the threshold, the following calculation was performed. A yield curve of the form $Y(E_b)=k(E_b-E_{th})^2+\bar{b}$ was assumed, where E_b and E_{th} are the betatron and threshold energies, respectively, $\bar{b}$ the average background, and k a constant factor. A table of random errors, $z_i=y_i/\sigma_i$, weighted according to the normal error distribution was evaluated. σ_i is the standard deviation in the measurement of y_i. To generate the yield curve, the same procedure as in the actual measurement was followed. One person selected an energy E_b and noted its corresponding yield, Y(true). Another person would read off z_i from the table of random errors. The measured yield at E_b was then given by

$$Y(\text{meas})=Y(\text{true})+\sigma_i z_i.$$

Fifty yield curves were generated and subjected to the

[9] A. G. W. Cameron, Atomic Energy of Canada Limited Report AECL-433, 1957 (unpublished).

same smoothing procedure to define the threshold. The resulting distribution for the threshold value obtained as a function of δ, the energy interval in which the yield curve was taken, is given in Fig. 3. The mean of the distribution deviates from the true value by 0.1δ. Thus, for a yield curve measured in intervals of 50 kev, we might expect a systematic error of the order of 5 kev. The standard deviation for a single observation is given by

$$\sigma_{s.d.}=[\textstyle\sum_i(T_i-\bar{T})^2/(n-1)]^{\frac{1}{2}}=0.72\delta$$

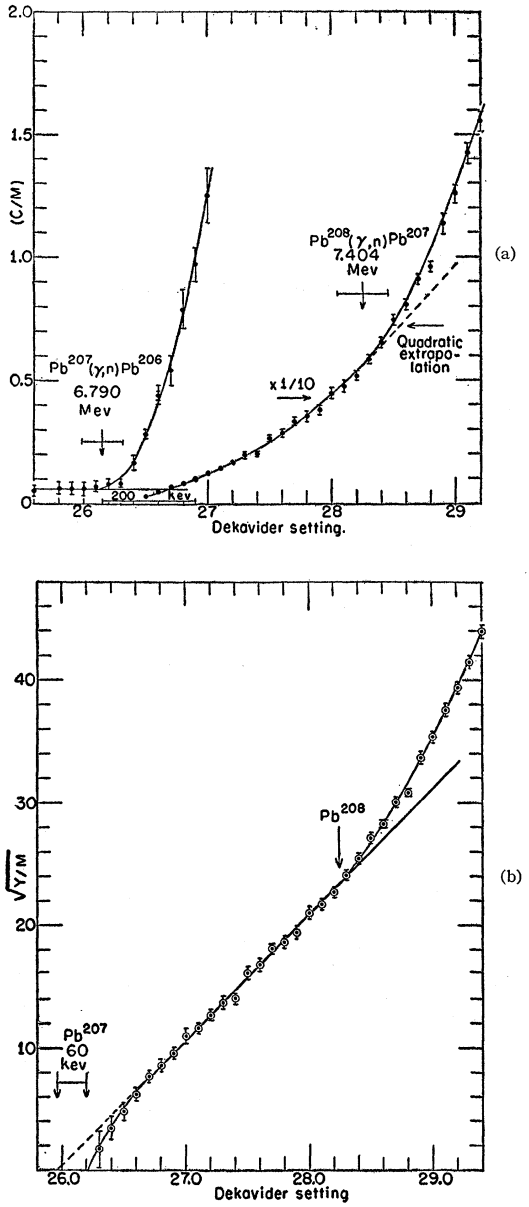

FIG. 2. (a) Neutron yield data for lead from 6.7 Mev to 7.7 Mev, and (b) square root plot of yield data. Linear extrapolation of $(Y/M)^{\frac{1}{2}}$ predicts an apparent threshold 60 kev lower than what is obtained from yield data in the immediate vicinity of threshold.

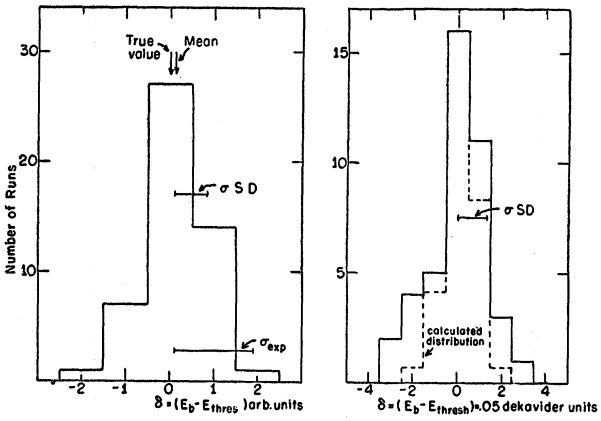

FIG. 3. (a) Calculated and (b) measured distribution of threshold values assuming a quadratic energy dependence for the yield curve, and visual extrapolation to define the threshold.

where $\bar{T}$ is the mean of n measurements T_i. The experimental estimate for the threshold uncertainty is 1.84δ. This indicates that the experimental uncertainty assigned to the quoted threshold values is indeed conservative. A comparison of the calculated and measured distribution obtained from 42 bismuth measurements is given in Fig. 3.

BETATRON ENERGY CALIBRATION

The peak bremsstrahlung energy is determined by the "integrator method" [1,10] where orbit expansion is made to occur at a preselected magnetic flux density. Modifications in circuit design and choice of analogue voltage representing the instantaneous electron momentum have led to improved energy stability and linearity of the betatron energy scale. Technical details of the energy control system and its performance will appear elsewhere.[11]

Calibration of the energy scale is based on the measurement of photoneutron thresholds for D^2(2.226 $\pm$0.001 Mev),[12] Bi^{209}(7.43$\pm$0.05 Mev),[13] Cu^{63}(10.826 $\pm$0.018 Mev),[14] and the threshold for detection of gamma rays elastically scattered from the 15.116$\pm$0.006 Mev[15] level in C^{12}. Assuming a linear energy scale of the form.

$$v^*=Ap+B$$

the parameters A and B are evaluated by a weighted least squares fit of the threshold data where both variables, v^* and p, are subject to error. v^* represents

[10] L. Katz et al., Can. J. Phys. **A38**, 113 (1950).
[11] K. N. Geller and E. G. Muirhead, Rev. Sci. Instr. (to be published).
[12] J. Mattauch, L. Waldmann, R. Bieri, and F. Everling, *Annual Review of Nuclear Science* (Annual Reviews, Inc., Palo Alto, 1956), Vol. 6. p. 179.
[13] J. R. Huizenga, Physica **21**, 410 (1955).
[14] K. S. Quisenberry, T. T. Scolman, and A. O. Nier, Phys. Rev. **104**, 461 (1956).
[15] R. W. Kavanagh and C. A. Barnes, Phys. Rev. **112**, 503 (1958).

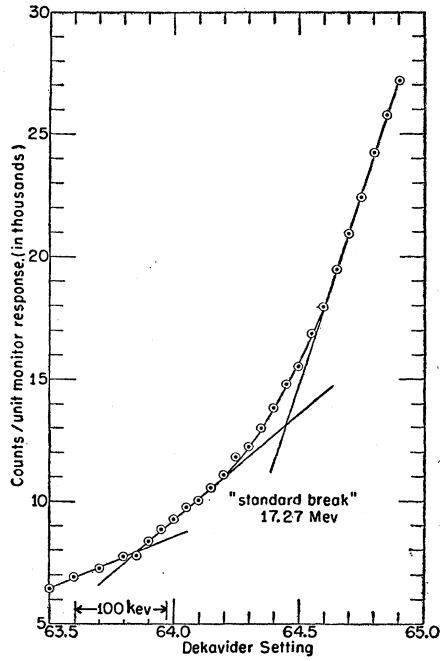

FIG. 4. Standard oxygen break at 17.27 Mev.

the potentiometer setting (Dekavider) corrected for finite time delay in the production of the x-ray pulse, and p the corresponding threshold energy corrected for center-of-mass motion and expressed in momentum units of $2m_0c$. The uncertainty in the slope of the calibration is 0.15% and in the intercept 11 kev.

The least squares adjusted values for the bismuth and copper thresholds are 7.432±0.010 Mev and 10.833±0.017 Mev, respectively. If we base the calibration on the thresholds for deuterium and the 15.12-Mev isochromat, the threshold energies predicted for bismuth and copper are 7.438 and 10.846 Mev. These are consistent with the adjusted values and support a linear energy scale from 2 to 15 Mev.

Small energy shifts during a given threshold determination were measured by detecting the activity from the $O^{16}(\gamma,n)O^{15}$ reaction at 17.35 Mev. The slope of the yield curve at this energy is 1.4%/3 kev. Total counts greater than 10^4 were easily obtainable so that energy shifts of 3 kev were detectable. Long term energy stability was determined by measuring the position of a very strong break in the oxygen yield curve at 17.27 Mev (see Fig. 4). The energy assignment for the standard break is in good agreement with the value of 17.25±0.04 Mev reported by Penfold and Garwin[5] and with the excited state in O^{16} at 17.29 Mev observed in the $N^{15}(p,n)O^{15}$ reaction.[16] The position of the standard break during a given threshold run was determined from the slope and average value of the oxygen activity above the break. All thresholds were referred to the standard break at a Dekavider setting of 64.70 or 17.27 Mev. Corrections for shifts in the position of the standard oxygen break from run to run were applied to the measured thresholds. The uncertainty in this correction was of the order of ±5 kev, the short term energy stability. Threshold measurements of deuterium, bismuth, and manganese were repeated periodically to detect changes in the slope of the energy scale. During the period of one year, five calibration shifts with deviations of less than 1% were encountered; these shifts were measured to better than 0.15%. The experimental uncertainty assigned to the threshold energies includes all errors due to extrapolation, energy shift corrections, and calibration parameters.

RESULTS

The threshold energies observed in the present experiment are summarized in Table I, Column 3. The results are compared with other results for the reaction Q value in Column 4. The method used to obtain the reported Q value is listed in Column 5; $Q(\beta^+)$ and $Q(\beta^-)$ are the Q values for positron and beta decay, and $Q(\epsilon)$ a lower limit to the mass difference from electron capture. LSA denotes the least squares adjusted value evaluated from mass data tabulations based on analysis of reaction energies and mass measurements. The question mark (?) appearing for tellurium indicates uncertainty in isotopic assignment. In some instances, where the transition is not to the ground state but to a known excited state of the residual nucleus, the neutron binding energy inferred from the present measurement is indicated in parenthesis below the quoted value. Otherwise, the observed threshold represents an upper limit to the neutron binding energy and is indicated by ($\leqslant$).

DISCUSSION

Systematic discrepancies occur between the observed threshold energies and Q values predicted by mass data where the difference in spin for ground-state transitions is $\geqslant 7/2$. Under such circumstances, neutron emission is suppressed at the true threshold, and the observed threshold represents either decay to excited states in the residual nucleus, or excitation energy at which the emitted neutron may overcome the angular momentum barrier with a reasonable probability.[2,17] Comparison of the observed threshold energies with mass data Q values for transitions having a spin difference $\geqslant 7/2$ are presented in Table II. The thresholds for Nd^{145}, Sm^{149}, Er^{167}, Hf^{179} and Hf^{180}, are consistent with transitions to known excited states in the residual nucleus. The large uncertainty in the mass data Q value for Y^{89} and In^{115} does not allow any definite conclusion to be made. However, the threshold ob-

[16] K. W. Jones, L. J. Lidofsky, and J. L. Weil, Phys. Rev. **112**, 1252 (1958).

[17] P. Axel, J. D. Fox, and R. H. Parker, Phys. Rev. **97**, 975 (1955).

TABLE II. Comparison of measured threshold energies with neutron binding energies predicted by mass data for transitions with $\Delta I \geq 7/2$. All energies in Mev.

Reaction	ΔI[a]	Observed threshold	Mass data Q value	$E_{th}-Q$	Excited state energy
$Cr^{52}(\gamma,n)Cr^{51}$	7/2	12.18±0.14	12.053±0.004[b]	0.13±0.14	...
$Y^{89}(\gamma,n)Y^{88}$	7/2	11.59±0.08	11.53 ±0.40[c]	0.06±0.41	0.387[d]
$In^{115}(\gamma,n)In^{114}$	7/2	9.22±0.03	9.35 ±0.43[c]	−0.13±0.43	0.191[a]
$Ce^{142}(\gamma,n)Ce^{141}$	(7/2)[e]	7.24±0.07	6.97 ±0.07[f]	0.27±0.10	...
$Nd^{145}(\gamma,n)Nd^{144}$	7/2	6.38±0.16	5.97 ±0.19[f]	0.41±0.25	0.690[a]
$Sm^{149}(\gamma,n)Sm^{148}$	7/2	6.45±0.16	5.87 ±0.28[f]	0.58±0.33	0.562[a]
$Er^{167}(\gamma,n)Er^{166}$	7/2	6.65±0.08	6.45 ±0.06[g]	0.20±0.10	0.081[a]
$Hf^{177}(\gamma,n)Hf^{176}$	7/2	6.69±0.03	6.28 ±0.06[g]	0.64±0.07	0.088[a]
$Hf^{179}(\gamma,n)Hf^{178}$	9/2	6.31±0.07	6.17 ±0.06[g]	0.14±0.09	0.093[a]
$Hf^{180}(\gamma,n)Hf^{179}$	9/2	7.85±0.11	7.32 ±0.06[g]	0.53±0.13	0.375[a]

[a] D. Strominger, J. M. Hollander, and G. T. Seaborg, Revs. Modern Phys. **30**, 585 (1958).
[b] C. F. Giese and J. L. Benson, Phys. Rev. **110**, 712 (1958).
[c] Henry E. Duckworth, *Mass Spectroscopy* (Cambridge University Press, New York, 1958), p. 177.
[d] S. Dzelepov and L. K. Peker, Atomic Energy of Canada Limited Report Tr. AECL-457 (unpublished).
[e] The discrepancy in the case of Ce^{142} predicts a ground-state spin for Ce^{142} of 0, since the spin of Ce^{141} is known to be 7/2.
[f] W. H. Johnson, Jr., and A. O. Nier, Phys. Rev. **105**, 1014 (1957).
[g] W. H. Johnson, Jr., and V. B. Bhanot, Phys. Rev. **107**, 6 (1957).

served for In^{115} is in excellent agreement with the value reported by Bendel et al.[3] for transitions to the isomeric state of In^{114}, 191 kev above its ground state. If the observed thresholds for Cr^{52} and Ce^{142} do correspond to excited state transitions, the present results indicate states in Cr^{51} and Ce^{141} at 130 and 270 kev, respectively. The large discrepancy for Hf^{177} cannot be explained on the basis of excited state transitions.

Several threshold results merit special treatment and are discussed below.

Al^{27}

The neutron yield data for $Al^{27}(\gamma,n)Al^{26}$ obtained with about 250 grams of aluminum ingot is shown in Fig. 5. The average of two separate measurements gives 13.26±0.07 Mev for the threshold energy. The Q value predicted from the reaction cycle

$Si^{29}(d,\alpha)Al^{27}$	5.994±0.011 Mev[18]
$+Si^{28}(d,p)Si^{29}$	6.246±0.010 Mev[18]
$-Si^{28}(d,\alpha)Al^{26}$	1.428±0.004 Mev[19]
$-D^{2}(\gamma,n)H^{1}$	2.226±0.001 Mev[12]

is 13.038±0.015 Mev. This result is consistent with the Q value of 13.06±0.01 Mev calculated from the (Al^{27},Mg^{26}) mass difference,[20] and the $Al^{26}(\beta^{+})Mg^{26}$ beta decay energy.[21] The 224±76 kev discrepancy between the observed threshold energy and the predicted Q value indicates that the reaction leaves Al^{26} in its excited state 228 kev above its ground state. Since the ground-state spin of Al^{27} is $5/2^{+}$, neither decay to the residual ground state of 5^{+} or to the 0^{+} excited state is favored. One would therefore expect the observed threshold to correspond to the ground-state Q value. To explain this anomaly, one might appeal to an isotopic spin selection rule. If we assume the photon interacts directly with the odd $d_{5/2}$ proton in Al^{27}, then the compound state will be $T=3/2$ if the absorption is predominantly electric dipole. The single particle proton state of Al^{27*} will be either $p_{3/2}$ or $f_{7/2}$. Conservation of isotopic spin will suppress neutron decay to the $T=0$ ground state of Al^{26}; transitions to the $T=1$ excited state will be allowed if Al^{27*} is in a $p_{3/2}$ state.

P^{31}

The activation curve for $P^{31}(\gamma,n)P^{30}$ shown in Fig. 6 was obtained with approximately 60 grams of red amorphous phosphorus tightly packed in plastic cylinders $1\frac{1}{4}$-in. diameter×$2\frac{1}{2}$ in. Activity counts were recorded for 300 seconds after a fixed delay of 40 seconds following the irradiation. The average value for the threshold energy, based on five determinations,

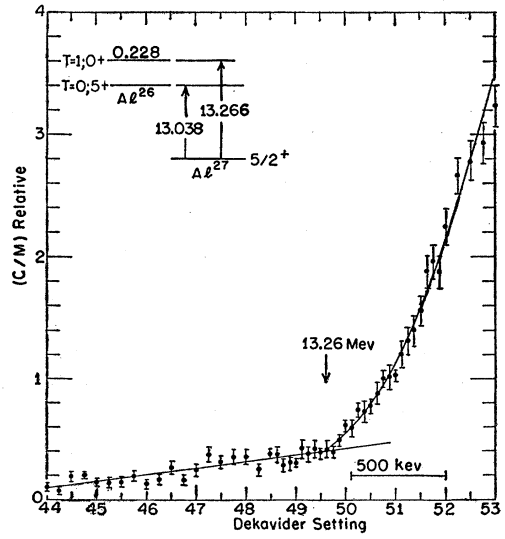

FIG. 5. Neutron yield data for aluminum from 11.8 Mev to 14.2 Mev.

[18] P. M. Van Patter and W. Whaling, Revs. Modern Phys. **26**, 402 (1954); **29**, 756 (1957).
[19] C. P. Browne, Phys. Rev. **114**, 807 (1959).
[20] T. T. Scolman, K. S. Quisenberry, and A. O. Nier, Phys. Rev. **102**, 1076 (1956).
[21] L. J. Lidofsky, Revs. Modern Phys. **29**, 773 (1957).

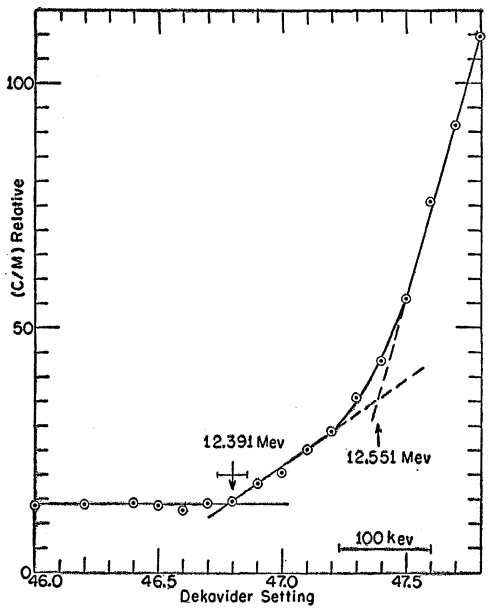

FIG. 6. Activation curve for phosphorus from 12.18 Mev to 12.66 Mev. Change in slope at 12.55 Mev is attributed to a level in the (γ,n) cross section at 12.59 Mev of width about 80 kev.

is 12.391±0.026 Mev. Because of the rather large discrepancies between the Q values predicted from mass data and reaction energies as indicated in Table I, it is difficult to give a definite interpretation to the observed threshold. The shape of the activation curve near threshold indicates the presence of fine structure in the phosphorus (γ,n) cross section. Thus, the observed threshold might correspond to resonant photon absorption rather than the true threshold, the cross section at threshold being too small to observe. Similarly the relatively sharp change in slope of the activation curve at 12.55 Mev indicates an excited state in P^{31} at about 12.59 Mev. The total width for this level is estimated to be 80 kev from the transition region between the two linear sections of the yield curve. Levels corresponding to these energies have not been previously reported.

The neutron binging energy for P^{31} is therefore $\leqslant$12.391 Mev. The value of 12.50±0.05 Mev reported by Chidley et al.[4] for the (γ,n) threshold of P^{31} is in better agreement with the energy assignment for the first break 0.16 Mev above the threshold.

K^{39}

The samples were compressed cylinders of potassium carbonate, 2-in. diameter by $1\frac{1}{2}$ in. thick and pressed under a pressure of 10 tons per square inch. The activation curve obtained by counting the annihilation radiation in coincidence is shown in Fig. 7. Activity counts were recorded for 600 seconds following a 50-second delay. The threshold energy for production of the 7.7 minute $T=0$, $J=3^+$ state of K^{38} is 13.125 ±0.038 Mev. This result, although higher than the Q value of 13.087±0.011 Mev reported by Giese and Benson,[22] is consistent with it within experimental errors.

The residual nucleus, K^{38}, belongs to the class of nuclei having odd-odd $N=Z$, and is of interest since it has more than one T value among its low-lying excited states.[23] However, the ordering of the $T=0$, $J=3^+$ and $T=1$, $J=0^+$ states is still uncertain. Stähelin,[24] on the basis of the positron decay energy for the 0.94-second $T=1$ state to the ground state of A^{38}, and the positron energy for decay of the 7.7-minute $T=0$ state to the 2.15-Mev state of A^{38}, concluded that the $T=0$ state was 0.39±0.30 Mev above the $T=1$ ground state. If this conclusion were correct, then the observed (γ,n) threshold energy detected by induced radioactivity from the 7.7-minute $T=0$ state would be 390 kev higher than the ground-state Q value. This, however, is not observed. The present results suggest that either (a) the $T=0$, 7.7-minute state is 38±40 kev above the $T=1$, 0.94-second ground state, or (b) the observed neutron separation energy does correspond to the ground-state Q value and the $T=1$ state is above the $T=0$ ground state.

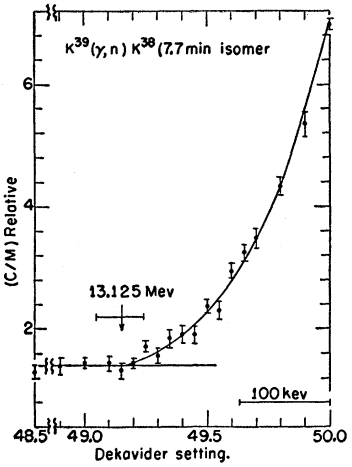

FIG. 7. Activation curve for the reaction $K^{39}(\gamma,n)K^{38}$ (7.7-min state) from 12.95 Mev to 13.35 Mev.

This conclusion is consistent with the results of Green and Richardson[25] who looked for an internal conversion line in the decay of K^{38} which would be present if the $T=1$, $J=0^+$ state were really the ground state as supposed by Stähelin. Observing no such line in their measurements, they concluded that the $T=1$ state must lie either above the $T=0^+$ state or not more than 80 kev below it. Recent measurements of the positron decay energies for the 0.94-second state and the 7.7-minute state place the $T=1$, state 0.22±0.11

[22] C. F. Giese and J. L. Benson, Phys. Rev. **110**, 712 (1958).
[23] S. A. Moskowski and D. C. Peaslee, Phys. Rev. **93**, 455 (1954); P. Stähelin, Phys. Rev. **92**, 1076 (1953).
[24] P. Stähelin, Helv. Phys. Acta. **26**, 691 (1953).
[25] D. Green and J. Richardson, Phys. Rev. **101**, 776 (1956).

Mev above the $T=0$ state[26] which is again contrary to the supposition of Stähelin.

Ta^{181}

The (γ,n) threshold for tantalum was measured by direct neutron detection and induced radioactivity. The neutron yield data obtained with 100 grams of tantalum foil is shown in Fig. 8. The threshold energy for the (γ,n) reaction is 7.640±0.025 Mev; this is the average value for five measurements.

Tantalum foils $1\frac{1}{4}$ in.×$1\frac{7}{8}$ in.×5 mil thick were irradiated 25 cm from the betatron target for about 20 minutes. The activation curve obtained for the production of the 8.1-hour isomeric state of Ta^{180} is also shown in Fig. 9, The threshold energy for the reaction $Ta^{181}(\gamma,n)Ta^{180m}$, based on two measurements, is 7.852±0.026 Mev.

The present results indicate that the 8.1-hour state

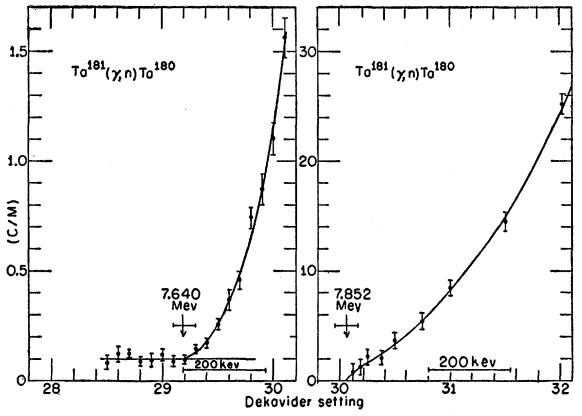

FIG. 8. Photoneutron yield curves for Ta^{181} measured by direct neutron detection and induced radioactivity. The difference in the observed thresholds indicates the 8.1-hr isomer to be 212 kev above the naturally occurring Ta^{180} ground state.

of Ta^{180} is an excited state of the naturally occurring long-lived Ta^{180} ground state. The excitation energy for the isomeric state is 212±33 kev. Previous attempts to determine whether naturally occurring Ta^{180} was the ground state or an isomer of the 8.1-hour Ta^{180} were made by detecting the radioactivity from natural Ta^{180}. A lower limit for the half-life of $(2.1\pm0.04)\times10^{13}$ years was reported for decay by K capture to the ground state of Hf^{180}, and $(1.7\pm0.03)\times10^{13}$ years for beta decay to the first excited state in W^{180}.[27] From the energy separation between the 8.1-hour isomer and the ground state of Ta^{180}, 212 kev, and the beta energy for decay to the 2^+ state in W^{180}, 605 kev, the energy available for beta decay from Ta^{180} ground state to the 2^+ state in W^{180} is 393 kev. The available beta-decay energy and the lower limit to the half-life

[26] P. M. Endt and C. M. Braams, Revs. Modern Phys. **29**, 683 (1957).

[27] E. R. Bauminger and S. G. Cohen, Phys. Rev. **110**, 953 (1958).

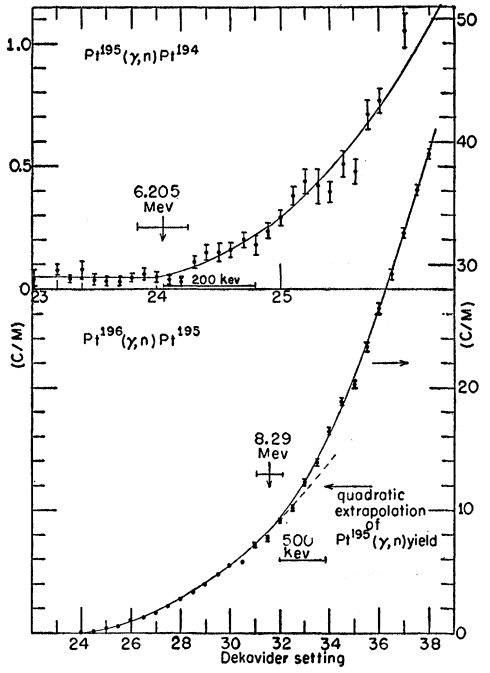

FIG. 9. Neutron yield data for platinum from 5.94 Mev to 9.96 Mev.

leads to a log ft value of about 21.2. This is associated with a fourth or fifth forbidden transition which places the spin of Ta^{180} at 6 or 7. This is consistent with the ground-state configuration of $h_{11/2}$ for the odd proton and $p_{3/2}$ for the odd neutron.

Pt^{195}; Pt^{196}

The neutron yield curve for platinum obtained with a 20-gram sample of platinum foil is shown in Fig. 9. The lowest threshold observed, at 6.205±0.044 Mev, is attributed to Pt^{195}. The threshold observed at 8.29±0.14 Mev is attributed to Pt^{196}. These results disagree with the Q values of 6.09±0.06 for Pt^{195} and

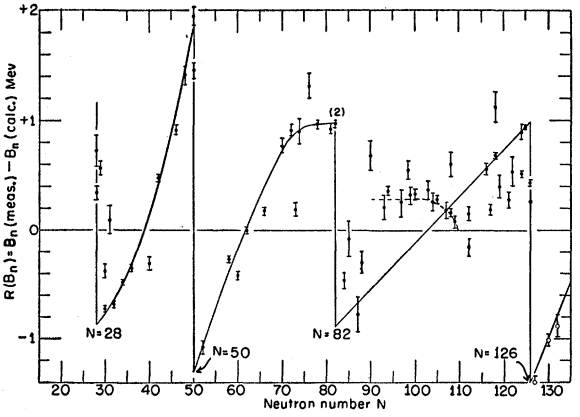

FIG. 10. Shell model corrections to the semiempirical mass formula.

TABLE III. Comparison of (γ,n) thresholds with (n,γ) Q values. All energies in Mev. Energies for excited states in platinum are taken from the decay schemes of Dzelepov and Peker.[a]

Reaction	Q, if (γ,n) assumed to be excited state	Measured Q	Q, if (n,γ) assumed to be excited state
$Pt^{195}(\gamma,n)Pt^{194}$	5.88±0.04	6.21±0.04	6.21±0.04
$Pt^{194}(n,\gamma)Pt^{195}$	6.07±0.04	6.07±0.04	6.20±0.04
$Pt^{196}(\gamma,n)Pt^{195}$	not unique	8.29±0.14	8.29±0.14
$Pt^{195}(n,\gamma)Pt^{196}$	7.92±0.01	7.92±0.01	8.27±0.01

[a] S. Dzelpov and L. K. Peker, Atomic Energy of Canada Limited Report Tr. AECL-457 (unpublished).

7.91±0.06 for Pt^{196} Mev obtained from mass measurements by Johnson and Bhanot.[28] The discrepancy of 0.12 Mev for Pt^{195} and 0.38 for Pt^{196}, cannot be explained in terms of excited state transitions. It is interesting to note that the Q values obtained from neutron capture data are also in disagreement with the present results to the same extent as the mass data. However, comparison of the two sets of results, (γ,n) and (n,γ), indicates that the measured (n,γ) Q values can be brought into agreement with the (γ,n) results if one assumes that ground state transitions were not measured in the neutron capture experiments. The reverse cannot be satisfied. This is indicated in Table III.

CONCLUSIONS

The neutron separation energies inferred from the present (γ,n) threshold measurements are compared with the values predicted from the semiempirical mass formula given by Fermi and tabulated by Metropolis and Reitwiesner[29] in Fig. 10. The difference between the measured and calculated values are plotted against neutron number N. The usual sharp discontinuities occur at the magic numbers $N=28$, 50, 82, and 126. To exhibit shell closure at $N=126$, the neutron separation energies for Bi^{210}, Po^{214}, and Po^{216} have been evaluated from the mass tables given by Huizenga. The shell corrections to the semiempirical mass formula exhibit a rather smooth dependence on N, increasing with N between closed shell nuclei in the regions $28<N<50$ and $50<N<82$. However, in the region $82<N<126$, the shell corrections are fairly constant and small, particularly in the region of deformed nuclei, $90<N<110$. This is consistent with the description of roughly uniformly spaced particle levels for deformed nuclei as given by Nilsson.[30]

[28] W. H. Johnson, Jr., and V. B. Bhanot, Phys. Rev. **107**, 6 (1957).

[29] N. Metropolis and G. Reitweisner, Atomic Energy Commission Report AECNP-1980, 1950 (unpublished).

[30] S. G. Nilsson, Kgl. Danske, Videnskab. Selskab, Mat.-fys. Medd. **29**, No. 16 (1955).